Broadband visible-to-telecom wavelength germanium quantum dot photodetectors

Stylianos Siontas,[1,a] Haobei Wang,[2] Dongfang Li,[1] Alexander Zaslavsky,[1,2] and Domenico Pacifici[1,2]
[1]School of Engineering, Brown University, 184 Hope St., Providence, Rhode Island 02912, USA
[2]Department of Physics, Brown University, 182 Hope St., Providence, Rhode Island 02912, USA

(Received 15 August 2018; accepted 6 October 2018; published online 30 October 2018)

Germanium (Ge) quantum dot (QD) photodetectors (PDs) were fabricated on Ge substrates exhibiting a broadband, visible to near-infrared (near-IR) photoresponse in the $\lambda = 400$–1550 nm range. Room-temperature responsivities (R_{sp}) up to 1.12 A/W and internal quantum efficiency IQE = 313% were obtained, superior to conventional silicon and germanium photodiodes. Noise analysis was performed at visible $\lambda = 640$ nm and telecom $\lambda = 1550$ nm wavelengths, both yielding room-temperature specific detectivity $D^* \simeq 2 \times 10^{10}$ cm $Hz^{1/2}$ W^{-1}. Lowering the operating temperature and incident power led to sharply enhanced performance, with $D^* = 1.1 \times 10^{12}$ cm $Hz^{1/2}$ W^{-1} and IQE = 1000% at T = 100 K for an incident power of 10 nW at $\lambda = 1550$ nm. Based on their simple fabrication and silicon technology compatibility, these Ge QD PDs represent a promising alternative for broadband, high-performance visible to near-IR detection. *Published by AIP Publishing*. https://doi.org/10.1063/1.5052252

Semiconductor photodetectors (PDs) are utilized in a plethora of applications ranging from smartphone CMOS cameras to optical fiber communications and photonic chips. Significant advantages arise by shrinking the active detector material down to the nanoscale, where quantum confinement and the consequent discretization of energy levels allow for lower dark current, greater tunability of wavelength detection, and higher internal gain. The optoelectronic properties of Si and Ge quantum dots (QDs) embedded in various oxide matrices have been extensively studied.[1,2] High-performance semiconductor QD PDs based on Si,[3,4] Ge,[5,6] Ge/Si,[7] InAs,[8,9] and PbS[10–12] have been reported, covering the visible and IR wavelength range. Previously, we reported PDs based on Ge QDs embedded in a SiO_2 matrix, fabricated on Si substrates, with spectral responsivities up to 4 A/W and high internal gain up to 700% in the $\lambda = 400$–1100 nm range.[13–16] However, those PDs were incapable of producing a significant photoresponse beyond $\lambda = 1100$ nm, corresponding to the Si substrate bandgap.[17] In this work, Ge QD PDs were fabricated on Ge substrates, extending the working spectral range up to the $\lambda = 1550$ nm telecom wavelength. These PDs exhibit a broadband, visible to near-IR photoresponse in the $\lambda = 400$–1550 nm range, with higher responsivity than both conventional Si and Ge photodiodes.

The fabrication process followed was the same as described in previous work,[15,16] but here Ge and SiO_2 targets were co-sputtered on *n*-Ge substrates so as to extend the photoresponse up to $\lambda = 1550$ nm, based on the fact that photon absorption takes place predominantly in the substrate, which in turn determines the PD's working spectral range.[13] The *n*-Ge substrates used were lightly doped ($\rho = 2.6\ \Omega$ cm) with the aim of minimizing recombination of photogenerated carriers and were kept at 400 °C during deposition. Adjusting the sputtering power and deposition time, PDs with QD layer thickness $W_{QD} = 160$ nm were obtained, as measured by profilometry and ellipsometry. This process yields QDs of ~2.5 nm mean diameter at a concentration of $\sim 2 \times 10^{19}$ cm^{-3} as obtained by transmission electron microscopy (TEM) analysis.[1,18] The samples were then annealed at 500 °C in a N_2 environment for 30 min, which generates larger size QDs with a ~4 nm mean diameter and a concomitant amorphous to crystalline phase transition.[1] Then, a $t = 100$ nm transparent, conductive indium-zinc-oxide (IZO) layer ($\rho = 0.001\ \Omega$ cm) was deposited as the top electrode. The light doping of the Ge substrate was designed to yield devices with a non-zero photoresponse in the visible range ($\lambda < 800$ nm) in contrast to conventional Ge *p*–*i*–*n* photodiodes, which suffer from Auger recombination in the heavily-doped *p*- or *n*-regions.[19] Photolithography was subsequently performed followed by etching in hydrofluoric acid to define 1.5 mm^2 area devices and suppress peripheral leakage current. Finally, the structure was completed by attaching the device to a sapphire substrate with a back indium contact.[15,16] The schematic geometry of the Ge QD PD structure is depicted in Fig. 1(a), whereas the energy band diagram including the corresponding interband optical transitions responsible for the photoresponse is provided in Fig. 1(b). The dashed red arrows depict the transport of electrons through the QD network via phonon-assisted tunneling, whereas the dashed green arrows depict the slower tunneling and subsequent trapping of holes in the QD surface states, leading to internal gain (see below for a detailed discussion of the gain mechanism).

The PDs were placed into a helium closed-cycle cryostat with optical access in order to obtain the temperature-dependent photoresponse. *I*–*V* measurements were performed scanning from −10 to 2 V with a measurement time of 1.6 s per voltage point. Incident light was provided by a super-continuum laser (SuperK EXTREME, NKT Photonics), coupled to a wavelength selector (SuperK VARIA, NKT Photonics) for individual

[a]Author to whom correspondence should be addressed: Stylianos_Siontas@brown.edu

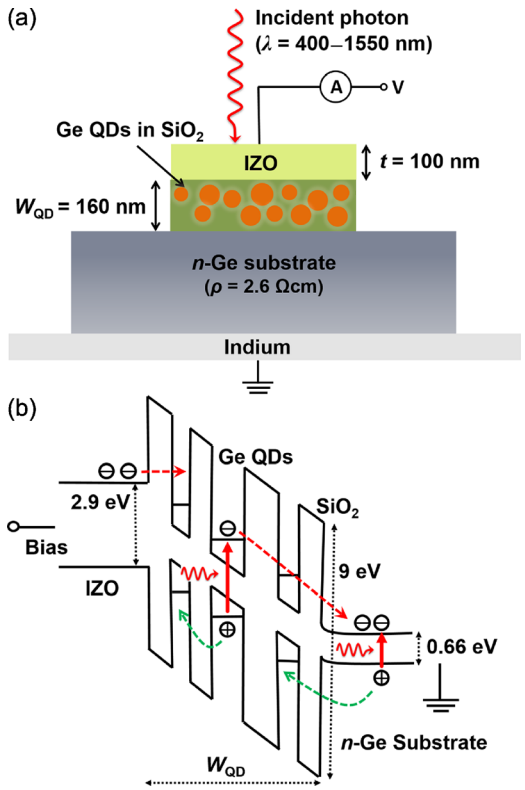

FIG. 1. (a) Schematic structure of a 1.5 mm^2 active area PD defined by photolithography, with $W_{QD} = 160$ nm and a $t = 100$ nm-thick IZO top electrode. (b) Schematic of the energy band diagram including the interband optical transitions responsible for the photoresponse (solid lines), with red dashed arrows depicting the electron transport via phonon-assisted tunneling and green dashed arrows depicting the slower tunneling and trapping of holes in QD surface states, leading to internal gain.[13–15]

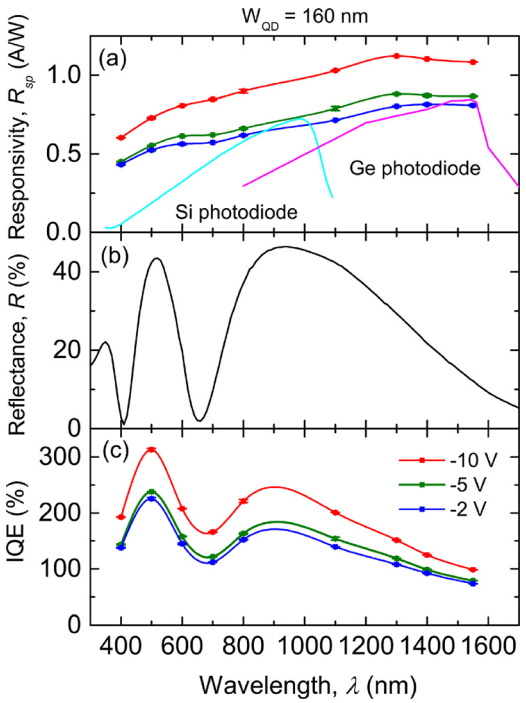

FIG. 2. (a) Responsivity (R_{sp}), (b) normal incidence reflectance ($R(\lambda)$), and (c) internal quantum efficiency (IQE) spectra of the Ge QD photodetectors at reverse biases of −10, −5, and −2 V. For panels (a) and (c), each point represents the mean value, whereas the (negligible) error bars represent the standard deviation of two separate measurement runs, inferring reproducible device behavior.

wavelength selection in the $\lambda = 400$–800 nm range, whereas narrow (FWHM = 10 nm) bandpass filters intercepting the beam were utilized to provide light in the $\lambda = 1100$–1550 nm range. The laser output was coupled to an optical fiber and was focused onto a ∼1 mm diameter spot on the PD active area at normal incidence. The optical power was tuned by using a neutral density wheel and measured by calibrated Si and Ge photodiodes.

The mean and standard deviation of the room-temperature responsivity $R_{sp}(\lambda)$ in Fig. 2(a) were obtained at various reverse bias voltages, namely, −10, −5, and −2 V by averaging two separate *I–V* measurement runs and dividing the photocurrent by the incident optical power (P_{in}).[15] The obtained R_{sp} at −10 V bias reaches a peak value of 1.12 A/W, superior to conventional Si and Ge photodiodes[19–21] as depicted by the cyan and magenta curves, respectively. The negligible error bars confirm that the device behavior is reproducible, whereas the absence of sharp absorption peaks is attributed to light absorption taking place predominantly in the Ge substrate[13] but also due to a dispersion of QD sizes and an abundance of surface states,[5] leading to a more uniform spectral responsivity. Even at −5 and −2 V, R_{sp} is still comparable to optimized Si and Ge photodiodes as a result of nearly-saturated behavior of the *I–V* curves in reverse bias (not shown here). The sample's normal incidence reflectance is presented in Fig. 2(b) measured using an QEX10 system from PV measurements including a xenon lamp and spectrograph for individual wavelength selection, as well as a calibrated reflection sample. It should be noted that the oxide layer is less insulating than a conventional silicon dioxide layer due to the presence of Ge QDs and defect states that are responsible for carrier transport, separation, and trapping, which eventually determine the high internal photoconductive gain. Moreover, the sample's absorption properties are influenced by thin-film interference effects which can be tailored by varying both W_{QD} and the IZO thickness t in order to optimize R_{sp}. Finally, the internal quantum efficiency (IQE) was calculated from Eq. (1) and is presented in Fig. 2(c). IQE is above 100% across the entire wavelength range as a result of the photoconductive gain mechanism present in the devices, reaching a maximum of 313% for −10 V reverse bias. It is also worth noting that IQE is >100% even at −5 and −2 V biases. The gain mechanism, as proposed in our previous work,[13–15] is the following: e-h pairs are photo-generated predominantly in the Ge substrate, with a smaller percentage generated in the Ge QDs, both via interband optical transitions as seen in the schematic band diagram shown in Fig. 1(b). Then, due to the large difference in effective mass, the holes tunnel exponentially slower than electrons and get trapped by the QD surface states [see dashed green arrows in Fig. 1(b)].[5] Consequently, a net positive charge accumulates in the QD layer, which attracts additional electrons from the IZO contact that transits through the oxide matrix via phonon-assisted tunneling, contributing to the observed photocurrent [see dashed red arrows in Fig. 1(b)]. The key contribution of the QDs to the gain mechanism, responsible for the high photoresponse, was verified by fabricating control devices possessing a QD-free SiO_2 layer which in turn did not exhibit any

mensurable photoresponse.[13] Additionally, the spectral shape of the IQE follows the reflectance $R(\lambda)$ since R_{sp} remains fairly constant

$$\mathrm{IQE}(\lambda) = \frac{hc}{\lambda e}\frac{R_{sp}(\lambda)}{1-R(\lambda)}. \quad (1)$$

Figure 2(c) also shows that the IQE falls off as λ increases into the near-IR regime. This is attributed to the longer wavelengths penetrating deeper into the Ge substrate since photogenerated holes that are produced more than a diffusion length away from the interface cannot reach the QD layer and contribute to the gain mechanism.[13,15] Furthermore, while IZO is fully transparent in the visible, it begins to absorb above $\lambda = 1300$ nm, such that a higher percentage of incident photons does not reach the Ge substrate.[22]

In order to characterize the power and temperature dependence of our PDs, the *I–V* characteristics were measured as a function of incident power P_{in} at room-temperature and at the cryogenic temperature of 100 K for a representative visible wavelength of 640 nm and the near-IR telecom wavelength of 1550 nm. A $R_L = 15\,\mathrm{k\Omega}$ resistor connected in series was used as a load. Figure 3 demonstrates the dependence of the photocurrent (I_{ph}) on P_{in} ranging from 10 nW to 12 μW for a reverse bias of −10 V. At T = 300 K, the photocurrent for both incident wavelengths increases linearly above 300 nW with that for $\lambda = 1550$ nm being slightly larger than for 640 nm illumination, in agreement with $R_{sp}(\lambda)$ presented in Fig. 2(a). For $P_{in} < 300$ nW, I_{ph} decreases sublinearly as the total current approaches the dark current. The linear dependence of I_{ph} on P_{in} above 300 nW implies a constant IQE, as shown in Fig. 3(b). It is noted here that for T = 300 K operation and $P_{in} < 100$ nW, the photoresponse is not discernible within a standard deviation of two consecutive separate *I–V* measurement runs as the total current is dominated by the dark current. For T = 100 K, I_{ph} shows a

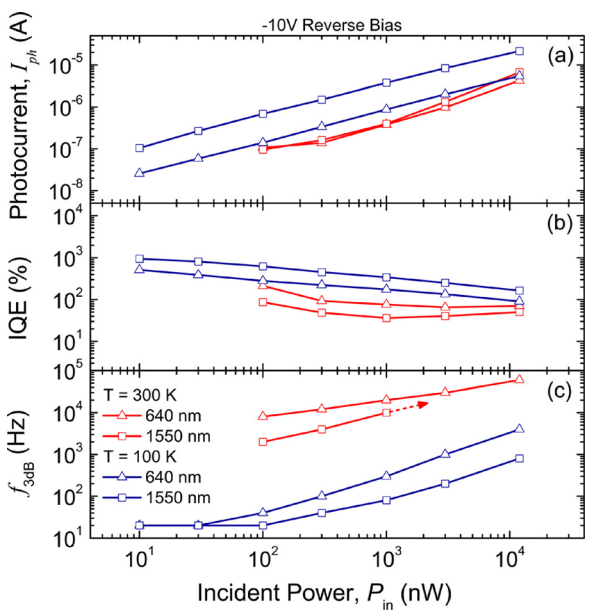

FIG. 3. Experimentally measured dependence of (a) the photocurrent (I_{ph}), (b) IQE, and (c) 3 dB bandwidth (f_{3dB}) on incident power (P_{in}) at operating temperatures of T = 300 K and T = 100 K at both visible ($\lambda = 640$ nm) and near-IR ($\lambda = 1550$ nm) illumination.

sublinear behavior across the entire incident power range for both illumination wavelengths, which is attributed to the saturation of the QD charging process and the reduction of available tunneling paths through the QD network as temperature is lowered, due to suppressed phonon-assisted tunneling.[16] The sublinear behavior of the photocurrent for T = 100 K at both λ results in an increasing IQE as P_{in} is reduced, reaching a maximum of 1000% for $\lambda = 1550$ nm at $P_{in} = 10$ nW.

The frequency response of the PD at the two operating temperatures was also obtained as a function of incident power at both visible and near-IR wavelengths under consideration. A digitally modulated diode laser with a rise time of <1.5 ns [23] was utilized to illuminate the sample at $\lambda = 640$ nm, whereas a mechanical chopper was utilized to modulate light at $\lambda = 1550$ nm from the super-continuum laser source. The 3 dB bandwidth (f_{3dB}) was measured via roll-off measurements of the voltage across R_L with the results presented in Fig. 2(c). At T = 300 K, f_{3dB} for $\lambda = 640$ nm increases sublinearly, reaching a maximum of 60 kHz at $P_{in} = 12\,\mu$W. For $\lambda = 1550$ nm illumination, the behavior of the frequency response is similar with values reaching 10 kHz at $P_{in} = 1\,\mu$W. Larger f_{3dB} values are expected at higher P_{in} but are not measurable due to limitations arising from the artificial rise time introduced by the mechanical chopper. Decreasing the temperature to T = 100 K strongly reduces the frequency response as a consequence of longer trapping and hopping times between QDs, reaching a maximum of 4 kHz and 800 Hz for $\lambda = 640$ nm and $\lambda = 1550$ nm, respectively. It is noted here that higher f_{3dB} values can be achieved by thinning down the QD layer and by decreasing the PD area so as to minimize the parasitic capacitance, leading to a lower RC circuit time constant, where R is the sum of the load R_L and the detector's intrinsic resistance.[14]

Proceeding to the noise performance of the Ge QD PDs, an important figure of merit to consider is the specific detectivity $D^* = (A)^{1/2}/\mathrm{NEP}$, where A is the photodetector area and NEP is the noise-equivalent-power normalized by the measurement bandwidth B (equal to 0.3 Hz for all measurements in this work). NEP provides a measure of the minimum optical power that can be detected by a photodetector and is equivalent to the P_{in} value that will generate I_{ph} equal to the thermal noise floor of the PD circuit (σ_{th}) for a measurement bandwidth $B = 1$ Hz, implying that $\mathrm{NEP} = \sigma_{th}/(R_{sp}\sqrt{B})$. The thermal noise consists of two components, namely, $\sigma_{th}^2 = (\sigma_j^2 + \sigma_d^2)$, where $\sigma_j^2 = 4kTB/R_L$ is the Johnson-Nyquist noise introduced by the thermal motion of charge within the load resistance R_L and k is the Boltzmann constant, whereas $\sigma_d^2 = 2e(BI_d\mathrm{IQE})$ is the dark current shot noise.[21] The dependence of σ_{th} on incident power and operating temperature was calculated in order to estimate D^* which is presented in Fig. 4(a) at −10 V reverse bias. At T = 300 K, for both $\lambda = 640$ and 1550 nm, $D^* \simeq 2 \times 10^{10}$ cm Hz$^{1/2}$ W^{-1} independent of P_{in}, as expected from Figs. 3(a) and 3(b) and Eq. (1). This D^* value is better or comparable to photodetectors reported for a similar wavelength and temperature in the literature based on Ge/Sn and Ge/graphene heterostructures as well as HgCdTe and organic molecules.[24–27] At T = 100 K, the detectivity shows up to

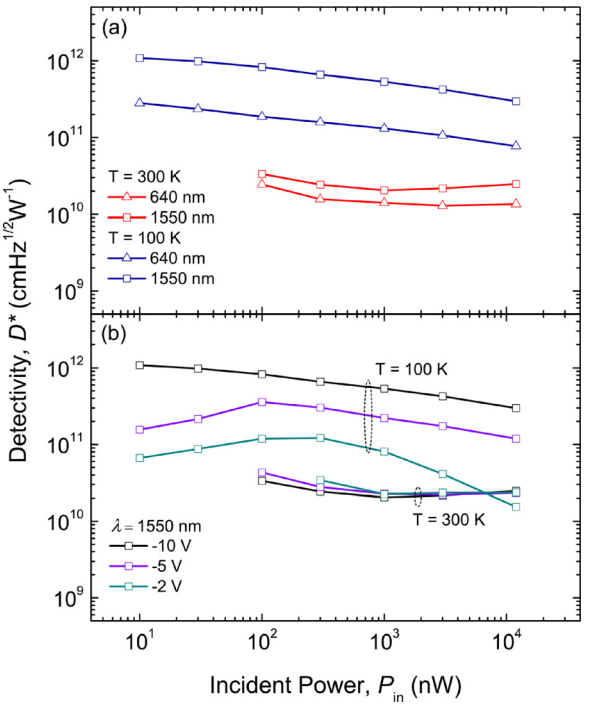

FIG. 4. (a) Specific detectivity (D^*) dependence on incident optical power (P_{in}) at T = 300 K and T = 100 K, for both visible ($\lambda = 640$ nm) and near-IR illumination ($\lambda = 1550$ nm) at −10 V of reverse bias. (b) D^* dependence on P_{in} as a function of reverse bias voltage for illumination at the $\lambda = 1550$ nm telecom wavelength.

two orders of magnitude enhancement with decreasing P_{in} as a direct consequence of increasing IQE. D^* reaches a maximum of 1.1×10^{12} cm Hz$^{1/2}$ W^{-1} for $\lambda = 1550$ nm at $P_{in} = 10$ nW, whereas for $\lambda = 640$ nm, $D^* = 3 \times 10^{11}$ cm Hz$^{1/2}$ W^{-1}. The lower D^* values in the visible are a consequence of the weaker photoresponse at $\lambda = 640$ nm.

Based on the results of Fig. 2, the Ge QD PDs are capable of operation at reverse bias voltages below −10 V while still retaining their high performance. For this reason, the dependence of D^* on P_{in} at both operating temperatures is provided in Fig. 4(b) for the technologically important $\lambda = 1550$ nm at three reverse bias voltages. At T = 300 K, D^* remains almost unchanged for −10, −5, and −2 V (it is noted that no measurable photoresponse was obtained at 100 nW for −2 V). As for T = 100 K, D^* increases for all reverse bias values as P_{in} is reduced down to 100 nW. Reducing P_{in} even further leads to suppressed D^* but remains above 10^{11} cm Hz$^{1/2}$ W^{-1} across all incident powers for −5 V reverse bias. For $P_{in} < 100$ nW, there is a trade-off between achievable D^* and low-voltage operation: when the reverse bias is reduced from −10 V to −2 V, D^* falls by approximately an order of magnitude, likely as a consequence of the weaker electric field, leading to a decreased tunneling probability through the Ge QD active region.

To summarize, we have demonstrated broadband Ge QD photodetectors fabricated on lightly-doped *n*-Ge substrates exhibiting a higher photoresponse than conventional Si and Ge photodiodes across the entire 400–1550 nm wavelength range at −10 V of reverse bias. Even when operated at lower bias, down to −2 V, our PDs are equal to or better than conventional Si or Ge photodiodes in terms of responsivity. As far as the noise performance is concerned, the PDs exhibit a constant room-temperature $D^* \simeq 2 \times 10^{10}$ cm Hz$^{1/2}$ W^{-1} for both visible $\lambda = 640$ nm and near-IR telecom $\lambda = 1550$ nm illumination. Operating at the cryogenic temperature of 100 K, the noise performance improves as incident power is lowered, resulting from the saturation of the QD charging process, leading to D^* enhancement up to almost two orders of magnitude. Specifically, at $P_{in} = 10$ nW, $D^* = 1.1 \times 10^{12}$ cm Hz$^{1/2}$ W^{-1}, and IQE = 1000%. As far as their frequency response is concerned, 3 dB bandwidth values up to 60 kHz were obtained, which can be further improved by minimizing the parasitics or reducing the QD active layer thickness. Based on their obtained figures of merit, the Ge QD PDs represent a promising alternative for broadband, visible to near-IR high performance photodetectors.

This work was supported by the National Science Foundation under Grant No. DMR-1203186. The Nanofabrication Central Facility (NCF) at Brown University is also gratefully acknowledged.

[1]S. Cosentino, S. Mirabella, M. Miritello, G. Nicotra, R. L. Savio, F. Simone, C. Spinella, and A. Terrasi, Nanoscale Res. Lett. **6**, 135 (2011).
[2]S. Ray, S. Maikap, W. Banerjee, and S. Das, J. Phys. D: Appl. Phys. **46**, 153001 (2013).
[3]J.-M. Shieh, W.-C. Yu, J. Y. Huang, C.-K. Wang, B.-T. Dai, H.-Y. Jhan, C.-W. Hsu, H.-C. Kuo, F.-L. Yang, and C.-L. Pan, Appl. Phys. Lett. **94**, 241108 (2009).
[4]J.-M. Shieh, Y.-F. Lai, W.-X. Ni, H.-C. Kuo, C.-Y. Fang, J. Y. Huang, and C.-L. Pan, Appl. Phys. Lett. **90**, 051105 (2007).
[5]S. Cosentino, E. Barbagiovanni, I. Crupi, M. Miritello, G. Nicotra, C. Spinella, D. Pacifici, S. Mirabella, and A. Terrasi, Sol. Energy Mater. Sol. Cells **135**, 22 (2015).
[6]S. Tzeng and P. Li, Nanotechnology **19**, 235203 (2008).
[7]R. Singha, S. Manna, S. Das, A. Dhar, and S. Ray, Appl. Phys. Lett. **96**, 233113 (2010).
[8]X. Lu, J. Vaillancourt, and M. J. Meisner, Appl. Phys. Lett. **91**, 051115 (2007).
[9]E.-T. Kim, A. Madhukar, Z. Ye, and J. C. Campbell, Appl. Phys. Lett. **84**, 3277 (2004).
[10]G. Konstantatos and E. H. Sargent, Nat. Nanotechnol. **5**, 391 (2010).
[11]J. P. Clifford, G. Konstantatos, K. W. Johnston, S. Hoogland, L. Levina, and E. H. Sargent, Nat. Nanotechnol **4**, 40 (2009).
[12]G. Konstantatos, I. Howard, A. Fischer, S. Hoogland, J. Clifford, E. Klem, L. Levina, and E. H. Sargent, Nature **442**, 180 (2006).
[13]S. Cosentino, P. Liu, S. T. Le, S. Lee, D. Paine, A. Zaslavsky, D. Pacifici, S. Mirabella, M. Miritello, I. Crupi *et al.*, Appl. Phys. Lett. **98**, 221107 (2011).
[14]P. Liu, S. Cosentino, S. T. Le, S. Lee, D. Paine, A. Zaslavsky, D. Pacifici, S. Mirabella, M. Miritello, I. Crupi *et al.*, J. Appl. Phys. **112**, 083103 (2012).
[15]S. Siontas, P. Liu, A. Zaslavsky, and D. Pacifici, Appl. Phys. Lett. **109**, 053508 (2016).
[16]S. Siontas, D. Li, P. Liu, S. Aujla, A. Zaslavsky, and D. Pacifici, Phys. Status Solidi A **215**, 1700453 (2018).
[17]See https://www.ioffe.ru for "Semiconductor Electronic Properties."
[18]S. Cosentino, S. Mirabella, P. Liu, S. T. Le, M. Miritello, S. Lee, I. Crupi, G. Nicotra, C. Spinella, D. Paine *et al.*, Thin Solid Films **548**, 551 (2013).
[19]See https://www.thorlabs.com for "Biased Si and Ge Detectors."
[20]A. Rogalski, *Infrared Detectors* (CRC Press, 2010).
[21]*Handbook of Lasers and Optics*, edited by F. Träger (Springer, 2012).
[22]A. Galca, G. Socol, and V. Craciun, Thin Solid Films **520**, 4722 (2012).
[23]See https://www.toptica.com for "iBeam Smart Diode Laser."
[24]N. Yahyaoui, N. Sfina, J. Lazzari, A. Bournel, and M. Said, Semicond. Sci. Technol. **30**, 085016 (2015).
[25]L.-H. Zeng, M.-Z. Wang, H. Hu, B. Nie, Y.-Q. Yu, C.-Y. Wu, L. Wang, J.-G. Hu, C. Xie, F.-X. Liang *et al.*, ACS Appl. Mater. Interfaces **5**, 9362 (2013).
[26]J. Wang, X. Chen, W. Hu, L. Wang, W. Lu, F. Xu, J. Zhao, Y. Shi, and R. Ji, Appl. Phys. Lett. **99**, 113508 (2011).
[27]J. D. Zimmerman, V. V. Diev, K. Hanson, R. R. Lunt, E. K. Yu, M. E. Thompson, and S. R. Forrest, Adv. Mater. **22**, 2780 (2010).